

End-to-End Quantum Machine Learning with Quantum Control Systems

Re-Bing Wu¹, Xi Cao¹, Pinchen Xie², and Yu-xi Liu³

Department of Automation, Tsinghua University, Beijing, 100084, China

Program in Applied and Computational Mathematics,

Princeton University, Princeton, NJ 08544, USA and

Institute of Micro-Nano Electronics, Tsinghua University, Beijing, 100084, China

(Dated: September 1, 2022)

This work presents a hardware-friendly end-to-end quantum machine learning scheme that can be implemented with imperfect near-term intermediate-scale quantum processors. The proposal transforms the machine learning task to the optimization of a quantum control system, which parameterize the learning model by experimentally tunable control variables. Our design also enables automated feature selection by encoding the raw input data to quantum states through agent control variables. Comparing with the gate-based parameterized quantum circuits, the resulting end-to-end quantum learning models is easy to implement as there are only few ad-hoc parameters to be determined by the designer. Numerical simulations on the benchmarking MNIST dataset without down-sampling the images demonstrate that the proposed scheme can achieve comparable high performance with only 3-5 qubits than known quantum machine learning models. The scheme is promising for efficiently performing larger-scale real-world learning tasks using intermediate-scale quantum processors.

Quantum Computing has entered the NISQ (Noisy Intermediate-Scale Quantum) era [1] in which it may surpass classical computing with even imperfect quantum hardware [2]. As one of its most promising applications, quantum machine learning is drawing intense attention [3, 4] for its potential supremacy on solving large-scale real-world learning tasks with quantum computers. Many algorithms have been proposed along this route, e.g., quantum supporting vector machine for classification problems [5], quantum principal component analysis [6] and quantum generative adversarial learning [7, 8].

To enable quantum machine learning algorithms on NISQ processors, a popular approach is to construct quantum neural-network (NN) models with parameterized quantum circuits (PQC) [9, 10] that is trained by classical optimization algorithms. Such hybrid quantum-classical models have universal approximation capabilities and are able to achieve classically intractable feature learning tasks [11]. Various applications have been put forward for quantum simulation of molecules [12], combinatorial optimization [13] and machine learning problems [14].

The PQC-based machine learning has also been experimentally demonstrated by shallow circuits on NISQ processors (with no greater than 20 qubits) [10] on classification [15], clustering [16] and generative [17] learning tasks. To our knowledge, few of them were tested with real-world datasets, and the achieved performance is still far below classical algorithms. For the benchmarking example of the MNIST dataset [18] for recognition of hand-written digits, the precision of classification is no higher than what can be achieved by a simple classical logistic regression model, and in most cases the

original images have to be down-sampled to make compromises with scarce quantum resources (e.g. limited number of qubits and decoherence time).

On top of limited quantum resources, the architecture of current PQC ansatz also challenges the development of practical NISQ processors, because the gate sequences used in PQC cannot be trivially implemented by available quantum hardware with high fidelity. In other words, the circuit topology of a PQC is not fully compatible with actual controlled physical system, on which some unitary transformations are difficult to realize due to sparse qubit-qubit connectivity.

Moreover, as one of the most important characteristics of modern deep learning, a successful model should be capable of learning effective representation of the raw data. In quantum machine learning, a powerful automatic feature-selection encoder is hence highly desirable, as is recently proposed by the quantum kitchen sink [19] or quantum metric learning [20], to compress and better fit the input data for the selected quantum ansatz.

All these demands call for a hardware-friendly quantum machine learning scheme that can be efficiently deployed on NISQ processors. Ideally, the scheme should provide an end-to-end data pipeline that yields learning output from the input data with as less as possible hand-designed modules, and the entire physical implementation should be straightforward with only few ad-hoc elements/parameters to be selected.

To arrive at such an end-to-end quantum machine learning scheme, let us consider a classification learning task with a set of Z training samples $(x^{(k)}, y^{(k)})$, where $x^{(k)} \in \mathbb{R}^d$ is the input data represented by d -dimensional vectors and

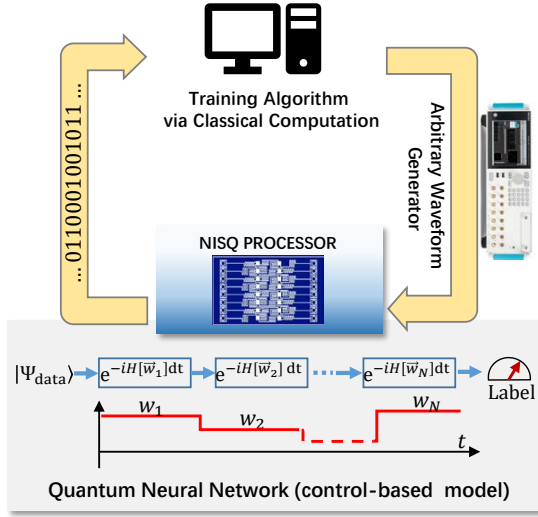


FIG. 1: The physical control flow of a hybrid quantum-classical algorithm deployed on a NISQ processor. The arbitrary waveform generator (AWG) produces control pulses that manipulate and measure the qubits on the processor. According to the qubit measurement outcomes, the classical computer runs the training algorithm to instruct the AWG to iteratively update the control pulses. The controlled quantum evolution forms a quantum NN parameterized by the time-dependent AWG parameters.

$y^{(k)} \in \{1, \dots, L\}$ is the corresponding label. For any PQC-based machine learning model, the input x is transferred to the quantum state $|\Psi(x)\rangle$ through some encoder circuit. After being processed by a succeeding quantum circuit represented by a parameterized unitary transformation $U(\mathbf{w})$, the output state is measured under a POVM measurement $\{M_1, \dots, M_L\}$, in which each operator M_k is associated with one class to be discriminated. The conditional probability of obtaining y for a given input x and circuit $U(\mathbf{w})$ is then defined as $P(y|x, \mathbf{w}) = \langle \Psi(x) | U^\dagger(\mathbf{w}) M_y U(\mathbf{w}) | \Psi(x) \rangle$, based on which the empirical loss is defined as follows:

$$L[\mathbf{w}] = 1 - Z^{-1} \sum_{k=1}^Z P(y^{(k)}|x^{(k)}, \mathbf{w}). \quad (1)$$

The PQC is known as a black-box model with tunable parameters associated with layered one-qubit or two-qubit quantum gates. Physically, the assigned two-qubit gates may have to be realized through a series of intermediate operations (e.g., SWAP) due to the lack of direct interactions between the target qubits. Thus, the actual compiled quantum circuit is usually deeper than the designed circuit.

From circuit model to control model - Let us take a closer look at an experimental superconducting

quantum computing system shown in Fig. 1 [21–23]. All gate operations in the PQC must be realized by shaped microwave pulses produced by an arbitrary waveform generator (AWG). These pulses are iteratively adjusted by a classical computer according to the empirical loss evaluated by measuring the control-guided output states. Thus, the entire PQC is in fact dictated by the AWG control pulses, whose amplitudes parameterize a new quantum NN realized by the controlled quantum dynamics. In this way, we can replace the gate-based model by a control-based model.

Interestingly, the control-based model also has a layered feedforward network structure owing to the piecewise-constant characteristic of AWG pulses. Ideally, the steering process of these pulses on the quantum system can be characterized by the Schrödinger equation:

$$|\dot{\Psi}(t)\rangle = -i \left[H_0 + \sum_{\ell=1}^M w_\ell(t) H_\ell \right] |\Psi(t)\rangle, \quad (2)$$

where $|\Psi(t)\rangle$ is the quantum state (starting from an initial state $|\Psi(t_0)\rangle = |0\rangle$) of the entire system, and $w_1(t), \dots, w_m(t)$ are the amplitudes of the control fields. Each control field consists of M piecewise-constant sub-pulses over M sampling periods. The states $|\Psi(t_k)\rangle$ at the end of each sub-interval form a layer of the quantum NN, and the control variables denoted by

$$\vec{w}_k = [w_1(t_k), \dots, w_M(t_k)], \quad k = 1, \dots, N, \quad (3)$$

are the equivalent NN hyper-parameters as schematically shown in Fig. 1. The depth of the quantum NN is equal to the number of AWG sampling periods during the entire quantum evolution.

The control-based model is a generalization of the gate-based model because any gate operation must be eventually realized through physical control pulses. Comparing with the gate-based PQCs, it is hardware more friendly because all parameters are directly adjustable without having to be artificially split into separate gates.

From hand-designed to auto-selected features - In most PQC-based learning models, the data vector is mapped to the quantum state using a pre-selected encoder to represent the set of hand-designed features. As schematically shown in Fig. 2(a), the same strategy can be applied as well in control-based models. The encoder first ‘translates’ the data vector to a quantum state, following which a physical control is applied to prepare the system in this state. The applied control could be very difficult to design when the encoded states are highly entangled (e.g., in the amplitude encoding scheme for exploiting the superposition of quantum states). The scheme also becomes impractical when dealing

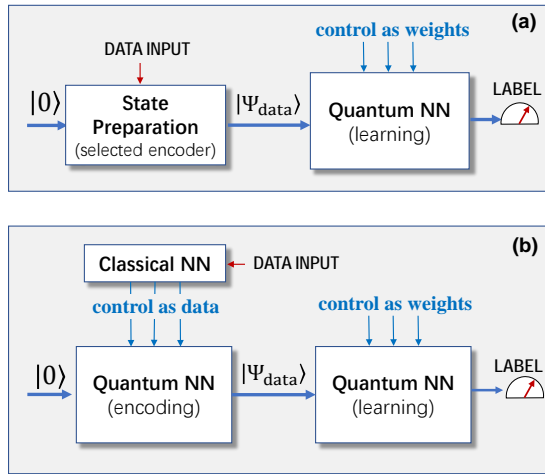


FIG. 2: Quantum end-to-end learning models that consist of encoding and inference control networks. (a) The data is encoded to the quantum state through a pre-selected encoder; (b) the data is encoded to the quantum state through a data-to-control interface (a classical NN) via a selected set of agent control variables. Following the encoding control processes, inference control pulses are applied as weights to infer the class that the input belongs to.

with large-size datasets because every single sample needs an individually designed control pulse.

We propose that the ‘translation’ from the data vector to the quantum state can be designed in an *implicit* and *automatic* manner. As is shown in Fig. 2(b), we introduce an intermediate data interface (e.g., a layer of classical perceptrons) that transforms the data vector into a selected set of agent control variables. The quantum state steered by these control variables then encodes the input data, but the encoded state is not explicitly (and neither necessarily) known unless being reconstructed through tomography.

In our encoding approach, the introduced data-to-control interface is to be trained together with the rest part of the quantum NN, forming a hybrid quantum-classical neural network. The selected encoding control variables act as a hidden layer that passes the input data from the classical computer to the quantum processor. Once the interface is well trained, control pulses will be automatically generated to prepare the target encoded state. In addition, the encoding scheme also brings favored nonlinearity through the nonlinear control-to-state mapping, which potentially leads to better model expressivity in complex learning tasks.

Training process - Now we have obtained an end-to-end learning model by control-based hybrid quantum-classical NNs. Suppose that the

involved control pulses contains M sampling periods, among which we assign the control variables $w^{\text{code}} = \{\vec{w}_1, \dots, \vec{w}_{M_0}\}$ in the first M_0 sampling periods as the agent hidden layer for encoding process, and $w^{\text{infer}} = \{\vec{w}_{M_0+1}, \dots, \vec{w}_M\}$ in the following sampling periods for the following inference process.

For illustration, the data-to-control interface is simply selected as a perceptron layer, i.e., each element of w^{code} is

$$w_i^{\text{code}} = B \cdot \frac{e^{\sum_j W_{ij} x_j + b_i} - 1}{e^{\sum_j W_{ij} x_j + b_i} + 1}, \quad (4)$$

where x_j is the j th element of the input data vector $x \in \mathbb{R}^d$, $W = \{W_{ij}\}$ and $b = \{b_i\}$ are the weight matrix and bias vector of the perceptrons, and $B > 0$ is the amplitude bound of the control variables. Because the bias term b can be merged into W by extending x to $(x^T, 1)^T$ and W to (W, b) , we will ignore b for simplicity. Thus, the hyper-parameters to be trained in the end-to-end model are $\mathbf{w} = (W, w^{\text{infer}})$.

The model is trained by minimizing the empirical loss $L[\mathbf{w}]$ defined by Eq. (1). Similar to most hybrid quantum-classical algorithms, these hyper-parameters are to be tuned along gradient-descent directions of the empirical loss. Since the gradient vector is not directly computable on the NISQ processors, we can sequentially perturb each hyper-parameter, measure the varied empirical loss and estimate the gradient of $\mathbf{w} = (W, w^{\text{infer}})$ via the finite difference:

$$\frac{\partial L}{\partial \mathbf{w}_j} \approx \frac{L(\mathbf{w} + \Delta \cdot \mathbf{e}_j) - L(\mathbf{w})}{\Delta}, \quad (5)$$

where \mathbf{e}_j is the unit vector along which only the j th element of \mathbf{w} is perturbed by Δ .

Let n be the number of qubits, and assume that each qubit is manipulated by two orthogonal control fields. Then we have $N_{\text{code}} = 2nM_0$ encoding control variables to be generated by $(d+1)N_{\text{code}}$ weight variables in W , and $N_{\text{infer}} = 2n(M-M_0)$ inference control variables to be directly tuned. Thus, we need to perform about $(d+1)N_{\text{code}} + N_{\text{infer}}$ ensemble measurements on the empirical loss $L[\mathbf{w}]$ to evaluate the gradient with respect to one input sample. The experimental overhead can easily exceed the ability of NISQ processors when the data space is high dimensional (e.g., when processing high-resolution images).

Nonetheless, observing that the gradient of the conditional probability $P(y|x, \mathbf{w})$ with respect to the entries of W can be decomposed (via chain rule)

Algorithm 1 Quantum End-to-End Learning

Input: training dataset $\{x^{(k)}, y^{(k)}\}$, the number m of control fields, batch size m (fixed or adaptive), learning rate α .

Output: the hyper-parameters $\mathbf{w} = (W, w^{\text{infer}})$ of the end-to-end learning model.

Initialize the classical NN weights W and inference control variables $w^{\text{infer}} = \{\vec{w}_{M_0+1}, \dots, \vec{w}_M\}$.

repeat

 Randomly pick a mini-batch of m samples from the training dataset.

for $i = 1$ **to** m **do**

 Feed the i th sample, say (\bar{x}, \bar{y}) in the batch to the perceptron layer weighted by W , which generates the encoding control variables $w^{\text{code}} = \{\vec{w}_1, \dots, \vec{w}_{M_0}\}$.

 Synthesize the control pulse with current w^{code} and w^{infer} .

 Perturbing the control variables one by one, and measure the gradients $\frac{\partial P(y|\bar{x}, \mathbf{w})}{\partial w^{\text{code}}}$ and $\frac{\partial P(\bar{y}|\bar{x}, \mathbf{w})}{\partial w^{\text{infer}}}$ along w^{infer} and w^{code} , respectively.

 Use $\frac{\partial P(\bar{y}|\bar{x}, \mathbf{w})}{\partial w^{\text{code}}}$ to compute the gradient $\frac{\partial P(\bar{y}|\bar{x}, \mathbf{w})}{\partial W}$ along W according to Eq. (6).

end for

 Compute the average gradient $\frac{\partial L[\mathbf{w}]}{\partial W}$ and $\frac{\partial L[\mathbf{w}]}{\partial w^{\text{infer}}}$ over the selected batch of samples, and make updates $W \leftarrow W - \alpha \cdot \frac{\partial L}{\partial W}$ and $w^{\text{infer}} \leftarrow w^{\text{infer}} - \alpha \cdot \frac{\partial L}{\partial w^{\text{infer}}}$, respectively.

until Empirical loss is sufficiently small

as:

$$\begin{aligned} \frac{\partial P(y|x, \mathbf{w})}{\partial W_{ij}} &= \frac{\partial P(y|x, \mathbf{w})}{\partial w_i^{\text{code}}} \frac{\partial w_i^{\text{code}}}{\partial W_{ij}} \\ &= \frac{\partial P(y|x, \mathbf{w})}{\partial w_i^{\text{code}}} \frac{B^2 - (w_i^{\text{code}})^2}{2B} x_j, \end{aligned} \quad (6)$$

where $1 \leq i \leq N_{\text{code}}$ and $1 \leq j \leq d + 1$, we only need to experimentally measure $\frac{\partial P(y|x, \mathbf{w})}{\partial w_i^{\text{code}}}$, while the rest parts is handled by a classical computer. The number of required ensemble experiments can thus be remarkably reduced from $(d+1)N_{\text{code}} + N_{\text{infer}}$ to $N_{\text{code}} + N_{\text{infer}}$ (the total number of control variables) that is not explicitly dependent on d .

Based on the measured gradient, we can apply the widely used stochastic gradient algorithms that are recently introduced to quantum robust control [24] and quantum approximate optimization algorithms [25]. Roughly speaking, in each iteration we randomly select a small batch of samples, apply the encoding and inference control fields, and measure the conditional probability $P(y|x, \mathbf{w})$ and its gradient for each sample. The averaged gradient over these samples is then used to update the model hyperparameters $\mathbf{w} = (W, w^{\text{infer}})$. The detailed pseudo-code of the optimization algorithm is shown in Algorithm 1.

Simulation results - Now we apply the proposed end-to-end learning model to the MNIST dataset for recognition of handwritten numbers. To demonstrate the effectiveness and efficiency, we use a simple chain systems of $3 \sim 5$ qubits, which are extensively used in solid-state quantum computing, as the physical realization of the NISQ processor. The Hamiltonian reads:

$$H(t) = \sum_{1 \leq i < n} g_{ij} \sigma_z^i \sigma_z^{i+1} + \sum_{k=1}^n [w_{kx}(t) \sigma_x^k + w_{ky}(t) \sigma_y^k] \quad (7)$$

where $\sigma_\alpha^k = \mathbb{I}_2 \otimes \dots \otimes \sigma_\alpha \otimes \dots \otimes \mathbb{I}_2$, $\alpha = x, y, z$, with σ_α being standard Pauli matrices. The neighboring qubit-qubit coupling strengths are $g_{12} = 1.5\text{MHz}$, $g_{23} = 2.0\text{MHz}$, $g_{34} = 2.5\text{MHz}$, and $g_{45} = 3.0\text{MHz}$, respectively. These qubits are addressed by control fields $w_{kx}(t)$ and $w_{ky}(t)$ along x -axis and y -axis, respectively. In the following simulations, we assume that the AWG sampling periods are all 5ns and the yielded controls are all bounded by $B = 25\text{MHz}$.

To train the learning model, we use 46993 samples belonging to 8 classes (the upper limit of 3-qubit models) corresponding to digits $\{0, 2, 3, 4, 5, 6, 8, 9\}$, and select the POVM measurement $\{M_j = |j\rangle\langle j|, j = 000, 001, \dots, 111\}$, where $\{|j\rangle\}$ (in binary representation) is the σ_z -basis of the first three qubits, to infer the discrimination result. The 28×28 -pixel sample images are converted to $d = 784$ dimensional vectors, and are fed into the data-to-control interface (a perceptron layer).

We first test learning models with fixed depth (all using 10 encoding layers and 10 inference layers) and variant number of qubits from 3 to 5, and an additional 3-qubit model with 50 coding layers and 50 inference layers to see whether deeper models can learn better. The learning curves (smoothed over the past 100 batches) in Fig. 3(a) show that the empirical loss can be reduced to below 10% after a few epochs (an epoch means the all training samples are traversed for once). The training performance is not significantly reduced by increasing the number of qubits (or equivalently the model width), but can be remarkably improved by increasing the number of AWG sampling periods, namely the depth of the quantum NN.

The generalizability of the trained end-to-end learning model is tested with the validation dataset (containing 7837 independent independent samples belonging to the 8 classes). Table I lists both the empirical loss evaluated on the validation dataset and the error rates evaluated by

$$R_{\text{error}} = P \left[\arg \max_y \langle \Psi_{x^{(j)}}(\mathbf{w}) | M_y | \Psi_{x^{(j)}}(\mathbf{w}) \rangle \neq y^{(j)} \right], \quad (8)$$

which is based on the inference rule that the label is inferred as y for input x if the probability of

TABLE I: Classification error rates on the validation MNIST dataset.

Model	Loss	Error Rate
3-QUBIT (10/10)	13.82%	8.15%
3-QUBIT (50/50)	9.56%	3.30%
4-QUBIT (10/10)	13.78%	8.18%
5-QUBIT (10/10)	14.06%	8.80%

producing y through the measurement is the largest. One can see from these indices that deeper model can significantly learn better than shallower models. The achieved performance is already close to those of classical NN models or quantum NN models. To our knowledge, such high performance (error rate lower than 10%) can only be obtained with PQC-based quantum machine learning models either on a reduced dataset (e.g., binary classification or with down-sampled images [14, 26, 27]) or with over 9 qubits [19, 28–30]. Therefore, our scheme is highly efficient when dealing with complex learning tasks.

Additional numerical experiments are carried out to further understand the respective roles of encoding and inference layers played in the end-to-end learning process. We first randomly pick a fixed W matrix and optimize the inference control variables. It turns out that the error rate can at most be reduced to around 30%. If we remove the inference control layers and train the encoding W alone, the error rate [see Fig. 3(b)] can be lowered to be under 10% with only 10 encoding control layers, and the performance can be further improved with deeper encoding networks. Then, we fix the trained W and investigate if the model can learn better with more inference control layers. The training results shown in Fig. 3(c) indicate that the error rate is not significantly reduced except when there are only few encoding layers, as is shown in. These tests are consistent with the practice of classical deep learning that the selection of features with the encoding control layers plays a more dominant role in the end-to-end learning process.

Figure 4 displays the optimized control pulses applied in the 3-qubit model. The controls in the first 50 sampling periods (blue) correspond to the encoding layers produced by the trained data-to-control interface from a randomly picked input sample. The controls in the following 50 sampling periods (red) correspond to the trained inference layers that are sample-independent. It is interesting that most coding control variables reach the set bound $B = 25\text{MHz}$, which is observed in almost all simulations. This pattern implies that the encoding control network may be further simplified (e.g., fix the control amplitudes and vary only the switching times), so that the model complexity can be

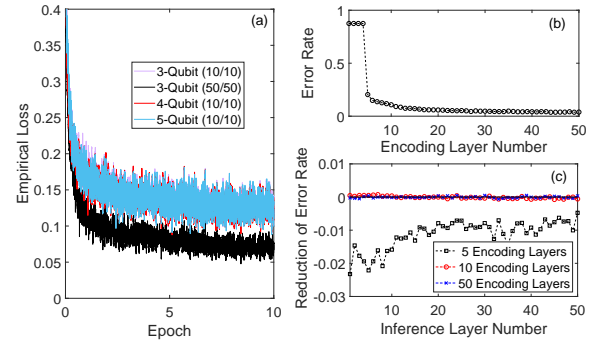


FIG. 3: The performance of the simulated quantum end-to-end learning processes. (a) the empirical loss during the training process for models with 3 ~ 5 qubits and different number of control layers; (b) the error rates of 3-qubit models without an inference network and 1 ~ 50 encoding layers; (c) the reduction of error rates of 3-qubit models using 1 ~ 50 inference layers, where the fixed 5-layer, 10-layer and 50-layer encoding networks are pre-trained in (b) with baseline error rates 20.38%, 10.78% and 3.87%, respectively.

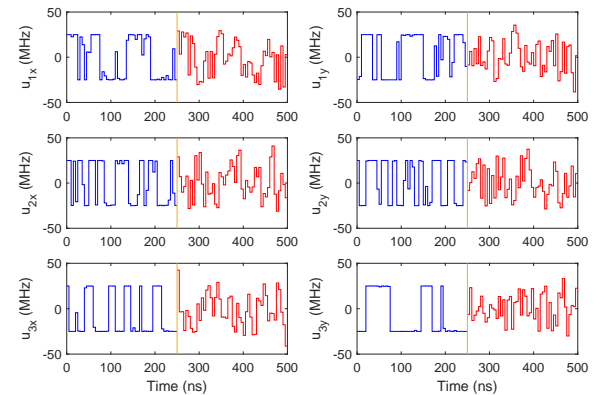


FIG. 4: The profiles of the control fields applied in the 3-qubit end-to-end learning model with 50 encoding layers generated from a random input sample (corresponding to 1 ~ 250ns containing 50 sampling periods) and 50 inference layers (corresponding to 251 ~ 500ns containing 50 sampling periods).

reduced. Moreover, the saturation of the encoding control amplitudes pulses can lead to the vanishing of gradients along the W variables, a common issue encountered in the practice of classical deep learning [31]. This problem should be resolved for further improving the performance.

Concluding remarks - To summarize, we proposed a hardware-friendly quantum end-to-end learning model that can be easily deployed on NISQ processors. The hybrid quantum-classical model involves quantum neural networks parameterized by experimental addressable control pulses, and

an embedded data-to-control interface for automatic feature selection. Numerical tests on the benchmarking MNIST dataset demonstrate that the model can efficiently achieve high performance with only a few qubit on real-world learning tasks without down-sampling the images. Taking into accounts of the precision, the size of dataset, and the model size, the scheme exhibits the best overall performance to our knowledge.

Our proposal turns the model training process into an optimal control problem, both of which can be resolved with gradient-descent algorithms. This interesting connection between optimal control and machine learning problems can be dated back to [32], where the famous BackPropagation algorithm was derived from foundational Pontryagin Maximum's Principle (PMP) in optimal control theory. Recently, it was rediscovered that PMP can be effectively applied to deep learning [33, 34], and from the opposite side, the design of robust quantum controls [24] and quantum optimizers [25, 35] can be taken as the design of a generalized learning model. We expect to develop more efficient and noise-resilient training algorithms from the unification of these two different but closely related fields.

From a control point of view, the capacity of the

quantum end-to-end learning model can be partially understood through the controllability of the underlying control system (i.e., the ability of generating arbitrary unitary transformations), which is is jointly determined by the connectivity of the physical qubit network, the bandwidth of the applied control fields (e.g., the sampling rate and the bound of control amplitudes) and the total time duration. The training of quantum machine learning models may also be easier, because the underlying quantum optimal control landscapes generically encounters no traps [36, 37]. Therefore, although quantum supremacy can be approached only with those transformations reachable in polynomial time [38], which seemingly does not require full controllability, we suggest that the selected physical quantum system should be as controllable as possible under admissible conditions, so as to facilitate the training of quantum machine learning models.

Finally, we indicate that the proposed quantum end-to-end learning scheme can be easily extended to NISQ processors containing larger number of qubits or other components (e.g., cavity modes or multi-level atoms). The framework is also transplantable to any other learning tasks. All these potentials will be explored in the future.

[1] J. Preskill, *Quantum* **2**, 79 (2018).

[2] F. Arute, K. Arya, R. Babbush, D. Bacon, J. C. Bardin, R. Barends, R. Biswas, S. Boixo, F. G. S. L. Bradao, D. A. Buell, et al., *Nature* **574**, 505 (2019).

[3] J. Biamonte, P. Wittek, N. Pancotti, P. Rebentrost, N. Wiebe, and S. Lloyd, *Nature* **549**, 195 (2017).

[4] V. Dunjko and H. J. Briegel, *Reports on Progress in Physics* **81**, 074001 (2018).

[5] P. Rebentrost, M. Mohseni, and S. Lloyd, *Phys. Rev. Lett.* **113**, 130503 (2014).

[6] S. Lloyd, M. Mohseni, and P. Rebentrost, *Nature Physics* **10**, 631 (2014).

[7] S. Lloyd and C. Weedbrook, *Phys. Rev. Lett.* **121**, 040502 (2018).

[8] L. Hu, S.-H. Wu, W. Cai, Y. Ma, X. Mu, Y. Xu, H. Wang, Y. Song, D.-L. Deng, C.-L. Zou, et al., *Science Advances* **5** (2019).

[9] D. Zhu, N. M. Linke, M. Benedetti, K. A. Landsman, N. H. Nguyen, C. H. Alderete, A. Perdomo-Ortiz, N. Korda, A. Garfoot, C. Brecque, et al., *Science Advances* **5** (2019).

[10] M. Benedetti, E. Lloyd, S. Sack, and M. Fiorentini, *arXiv preprint* (2019), arXiv:1906.07682.

[11] S. Lloyd, *arXiv preprint* (2018), arXiv:1812.11075.

[12] A. Kandala, A. Mezzacapo, K. Temme, M. Takita, M. Brink, J. M. Chow, and J. M. Gambetta, *Nature* **549**, 242 (2017).

[13] E. Farhi, J. Goldstone, S. Gutmann, and H. Neven, *arXiv preprint* (2017), arXiv:1703.06199.

[14] E. Farhi and H. Neven, *arXiv preprint* (2018), arXiv:1802.06002.

[15] V. Havlek, A. D. Croles, K. Temme, A. W. Harrow, A. Kandala, J. M. Chow, and J. M. Gambetta, *Nature* **567**, 209 (2019), ISSN 1476-4687.

[16] J. S. Otterbach, R. Manenti, N. Alidoust, A. Bestwick, M. Block, B. Bloom, S. Caldwell, N. Didier, E. Schuyler Fried, S. Hong, et al., *arXiv preprint* (2017), arXiv:1712.05771.

[17] K. E. Hamilton, E. F. Dumitrescu, and R. C. Pooser, *Phys. Rev. A* **99**, 062323 (2019).

[18] Y. LeCun, L. Bottou, Y. Bengio, and P. Haffner, *Proceedings of the IEEE* **86**, 2278 (1998).

[19] C. M. Wilson, J. S. Otterbach, N. Tezak, R. S. Smith, A. M. Polloreno, P. J. Karalekas, S. Heidel, M. S. Alam, G. E. Crooks, and M. P. da Silva, *arXiv preprint* (2018), arXiv:1806.08321.

[20] S. Lloyd, M. Schuld, A. Ijaz, J. Izaac, and N. Killoran, *arXiv preprint* (2020), arXiv:2001.03622.

[21] M. W. Johnson, M. H. S. Amin, S. Gildert, T. Lanting, F. Hamze, N. Dickson, R. Harris, A. J. Berkley, J. Johansson, P. Bunyk, et al., *Nature* **473**, 194 (2011).

[22] R. Barends, J. Kelly, A. Megrant, D. Sank, E. Jeffrey, Y. Chen, Y. Yin, B. Chiaro, J. Mutus, C. Neill, et al., *Physical Review Letters* **111**, 080502 (2013).

[23] X. Gu, A. F. Kockum, A. Miranowicz, Y.-x. Liu, and F. Nori, *Physics Reports* **718**, 1 (2017).

- [24] R.-B. Wu, H. Ding, D. Dong, and X. Wang, Phys. Rev. A **99**, 042327 (2019).
- [25] Y. Dong, X. Meng, L. Lin, R. Kosut, and K. B. Whaley, arXiv preprint (2019), arXiv:1911.00789.
- [26] E. Grant, M. Benedetti, S. Cao, A. Hallam, J. Lockhart, V. Stojanovic, A. G. Green, and S. Severini, npj Quantum Information **4**, 65 (2018).
- [27] W. Huggins, P. Patil, B. Mitchell, K. B. Whaley, and E. M. Stoudenmire, Quantum Science and Technology **4**, 024001 (2019).
- [28] I. Kerenidis and A. Luongo, arXiv preprint (2018), arXiv:1805.08837.
- [29] R. Sweke, F. Wilde, J. Meyer, M. Schuld, P. K. Fhrmann, B. Meynard-Piganeau, and J. Eisert, arXiv preprint (2019), arXiv:1910.01155.
- [30] M. Henderson, S. Shakya, S. Pradhan, and T. Cook, Quantum Machine Intelligence **2**, 1 (2020).
- [31] L. Bottou, F. E. Curtis, and J. Nocedal, SIAM Review **60**, 223 (2018).
- [32] Y. LeCun, in *The Connectionist Models Summer School* (1988), 1, pp. 21–28.
- [33] Q. Li, L. Chen, C. Tai, and E. Weinan, The Journal of Machine Learning Research **18**, 5998 (2017).
- [34] Q. Li and S. Hao, in *Proceedings of the 35th International Conference on Machine Learning*, edited by J. Dy and A. Krause (PMLR, Stockholm Sweden, 2018), vol. 80 of *Proceedings of Machine Learning Research*, pp. 2985–2994.
- [35] A. Dendukuri, B. Keeling, A. Fereidouni, J. Burbridge, K. Luu, and H. Churchill, arXiv preprint (2019), arXiv:1905.10912.
- [36] H. A. Rabitz, M. M. Hsieh, and C. M. Rosenthal, Science **303**, 1998 (2004).
- [37] R.-B. Wu, Q. Sun, T.-s. Ho, and H. Rabitz, Journal of Mathematical Chemistry **57**, 2154 (2019).
- [38] C. Arenz and H. Rabitz, Phys. Rev. Lett. **120**, 220503 (2018).